





# Electron transport parameters in CO<sub>2</sub>: A comparison of two experimental systems and measured data

## Journal Article

### Author(s):

Vass, Maté; [Egüz, Eda](#) ; [Chachereau, Alise](#) ; Hartmann, Péter; Korolov, Ihor; [Hösl, Andreas](#) ; Bošnjaković, Danko; Dujko, Saša; Donkó, Zoltán; [Franck, Christian](#) 

### Publication date:

2020-10

### Permanent link:

<https://doi.org/10.3929/ethz-b-000444490>

### Rights / license:

[Creative Commons Attribution-NonCommercial 4.0 International](#)

### Originally published in:

Journal of Physics D: Applied Physics 54(3), <https://doi.org/10.1088/1361-6463/abbb07>

# Electron transport parameters in CO<sub>2</sub>: A comparison of two experimental systems and measured data

Máté Vass<sup>1,2\*</sup>, Eda Egüz<sup>3</sup>, Alise Chachereau<sup>3</sup>, Péter Hartmann<sup>1,4</sup>,  
Ihor Korolov<sup>2</sup>, Andreas Hösl<sup>3</sup>, Danko Bošnjaković<sup>5</sup>, Saša Dujko<sup>5</sup>,  
Zoltán Donkó<sup>1</sup>, Christian M. Franck<sup>3</sup>

<sup>1</sup> Institute for Solid State Physics and Optics, Wigner Research Centre for Physics, H-1121 Budapest, Konkoly-Thege Miklós str. 29-33, Hungary

<sup>2</sup> Department of Electrical Engineering and Information Science, Ruhr-University Bochum, D-44780, Bochum, Germany

<sup>3</sup> Power Systems and High Voltage Laboratories, ETH Zurich, Physikstr. 3, 8092 Zurich, Switzerland

<sup>4</sup> Center for Astrophysics, Space Physics and Engineering Research (CASPER), Baylor University, 100 Research Pkwy, Waco, Texas, USA

<sup>5</sup> Institute of Physics, University of Belgrade, Pregrevica 118, 11080 Belgrade, Serbia

E-mail: [vass.mate@wigner.hu](mailto:vass.mate@wigner.hu)

Two experimental apparatuses used to obtain electron transport coefficients in gases are compared based on measurements in CO<sub>2</sub> over a wide range of  $E/N$ -values. The operation principles of the two experimental systems as well as their data acquisition methods are different. One operates under the Time Of Flight (TOF) principle, where the transport coefficients are obtained by fitting the theoretical form of the electron density of a swarm in an unbounded region,  $n(x, t)$ , to the measured current at different values of the drift length,  $I(L, t)$ . The other experimental apparatus operates in the Pulsed Townsend (PT) mode, where the electron transport coefficients are obtained by fitting the spatial integral of  $n(x, t)$  over the drift region to the measured, time-dependent current signal,  $I(t)$ . In both apparatuses, the measured  $E/N$  range was extended as much as possible to allow a large overlap for the comparison of the results. The bulk drift velocity,  $W$ , obtained by the two systems agrees well (within a few %) over a wide range of  $E/N$  values ( $100 \text{ Td} \leq E/N \leq 1000 \text{ Td}$ ). The agreement between the data sets for the longitudinal component of the bulk diffusion tensor,  $D_L$ , is less satisfactory, the TOF data show systematically higher values (by 10–50 % depending on  $E/N$ ) than the PT measurements. Significant differences are also found below 100 Td in case of the effective ionisation frequency,  $\nu_{\text{eff}}$ , and the (Steady State) Townsend ionisation coefficient,  $\alpha_{\text{eff}}$ , where the TOF apparatus is unable to give accurate results. Our comparison justifies the correctness of the measured data over the range of agreement and also indicates the interval in  $E/N$  where the data obtained by each of the experimental systems can be taken to be reliable. The limits of the operating regimes of the two setups, stemming from the hardware and from the physical limits, are discussed.

## 1 Introduction

Transport coefficients of charged particles in gases, besides having paramount importance in swarm physics, serve as fundamental input parameters for fluid modelling of gas discharges. In addition, they can be used to check and adjust cross section sets of different collision processes relevant for gas discharge physics, as transport coefficients can accurately be computed from the cross sections [1].

In order to improve plasma technologies, a thorough understanding of the chemical and physical processes present in the plasma phase is required, for which transport coefficients can be of use. As the most mobile charged particles are electrons in the plasma, accurate measurements of electron transport coefficients are crucial.

The gas investigated in this work, CO<sub>2</sub>, owing to its role in global warming, has been the subject of several research works, which mainly focus on its plasma-catalytic splitting into CO and O<sub>2</sub> [2–6], or its conversion into other valuable chemical compounds through e.g. a reaction with CH<sub>4</sub> (so-called dry reforming) [7–11]. Different types of plasma reactors have been applied for this purpose, e.g. dielectric barrier discharges (DBDs) [12–16], microwave plasmas [17–19], gliding arc [20–22] and spark discharges [23, 24]. The electron transport in CO<sub>2</sub> plays a key role in the optimization of non-equilibrium atmospheric pressure plasmas [25], in the modeling of production of oxygen in the atmosphere of Mars [26, 27] as well as in many studies of the CO<sub>2</sub> lasers [28] and particle detectors used in high energy physics [29].

The determination of transport coefficients has conventionally been based on *drift tube* measurements, where a low-density ensemble of electrons (an electron swarm) is created, which is subject to a homogeneous external electric field [30–32]. Based on their operation principles, we can distinguish between three major types of swarm experiments [33]:

- Time Of Flight (TOF) systems, where electron swarms are initiated by short pulses of an UV laser which hits a negatively biased electrode, thus emitting electrons through photoemission [31, 34, 35]. The system is equipped with a detector that collects "arriving" charges and gives a signal that is proportional to the number of these particles. In our previous works [42, 43] it has been assumed that the detected signal is (under hydrodynamic conditions) proportional to the spatio-temporal distribution of the density of the electron swarm,  $n(x, t)$  (see section 3 for definitions). From the functional form of  $n(x, t)$ , electron transport coefficients can be obtained through e.g. a fitting procedure.
- Pulsed Townsend (PT) systems [36–39], where the experimental realization is similar to that of a TOF system, but in this case the time-dependent displacement current generated by all the moving electrons within the whole electrode gap is measured at fixed electrode separation, i.e. the measured current  $I(t)$  is:

$$I(t) \propto \int_0^L n(x, t) dx, \quad (1)$$

where  $L$  is the electrode separation. The measurement can be repeated with different electrode separations. This way the consistency of the results can be checked. In a PT system, essentially the same transport coefficients can be obtained as in case of a TOF experiment.

- Steady State Townsend (SST) systems, where, unlike the two other types above, a steady stream of electrons is emitted from the cathode. At sufficiently large distances from the cathode, the following assumption can be made:

$$n(x) \propto e^{\alpha_{\text{eff}} x}, \quad (2)$$

where  $\alpha_{\text{eff}}$  is the effective ionization coefficient [40]. This transport coefficient can be determined by e.g. measuring the anode current at different gap distances. The other option under SST conditions would be the measurement of spatial profiles of emission that could be subsequently normalized at the anode to give spatially resolved net excitation rate. Such measurements in low current Townsend discharges allow a better understanding of various excitation mechanisms, including excitation by heavy particles and fast neutrals [41].

Assessing the accuracy of the measured coefficients is as important as the measured values themselves. Measurements obtained from a single experiment can only be evaluated with respect to their precision (which is related to the measurement scatter) but not with respect to their accuracy (i.e.

how well the measurements represent the true physical values). An estimation of the measurement accuracy can only be done via a detailed comparison with other measurements or with simulations. Such comparisons require detailed knowledge of the experimental conditions and data acquisition procedures for measurements (respectively simulation settings and underlying assumptions for simulations), in order to identify the cause of possible differences.

In this work, a comparison of measurements of electron transport coefficients in  $\text{CO}_2$  by two state-of-the-art experimental setups working under conceptually different principles and operating conditions, and using different data acquisition methods is presented. The transport coefficients investigated are the bulk drift velocity,  $W$ , the longitudinal component of the bulk diffusion tensor,  $D_L$ , the effective ionization frequency,  $\nu_{\text{eff}}$ , and the effective ionization coefficient,  $\alpha_{\text{eff}}$ . One of these setups is a ‘scanning’ drift tube apparatus [30], operating under TOF conditions, where a given electrode separation is scanned over, i.e. one measurement consists of a series of measurements at gap distances between a given minimum and maximum value, thus enabling the determination of the whole spatio-temporal distribution of the electron number density,  $n(x, t)$ . The other experimental system [36, 37] works under PT conditions, where for a given point in the parameter space,  $(p, U, L)$ , the displacement current from the electrons as well as the ions is measured. Here  $p$  is the pressure,  $U$  is the applied voltage and  $L$  is the electrode separation, which determine the reduced electric field ( $E/N$ ) value. By integrating the known analytic formula for  $n(x, t)$  (see section 2.2), the same transport coefficients can be determined as in case of the TOF system, thus enabling a direct comparison of two different techniques aiming to reach the same goal. To our knowledge, such a direct comparison has not yet been conducted for the experiments currently in active use. Thus, one of the main objectives of the present paper is to make comparisons between the two experimental systems using the measurements of electron transport coefficients in  $\text{CO}_2$ . This will allow us to assess the advantages and disadvantages of these two experimental systems, their accuracy and limits of applicability. The manuscript is structured as follows: In section 2 the experimental apparatuses and the related data acquisition methods are described in detail (in sections 2.1 and 2.2, respectively, for the Time Of Flight and Pulsed Townsend setups). A comparison of the two approaches is given in section 2.3. The experimental results are presented in section 3 and discussed in section 4 and finally, conclusions are drawn.

## 2 Description and comparison of the experimental systems and data acquisition.

Below, in sections 2.1 and 2.2 we provide a detailed description of both experimental setups and the specific data acquisition methods used. In section 2.3 a comparison of the two techniques is given.

### 2.1 The Time Of Flight experiment

#### 2.1.1 Description of the experimental setup

The Time Of Flight experiment is based on a ‘scanning’ drift tube apparatus, which has been presented in [30]. This apparatus has already been applied to measure transport coefficients of electrons in various gases: argon, synthetic air, methane, deuterium [42], carbon dioxide [43], acetylene ( $\text{C}_2\text{H}_2$ ), ethylene ( $\text{C}_2\text{H}_4$ ) and ethane ( $\text{C}_2\text{H}_6$ ) [44]. The simplified scheme of the experimental apparatus is shown in Figure 1.

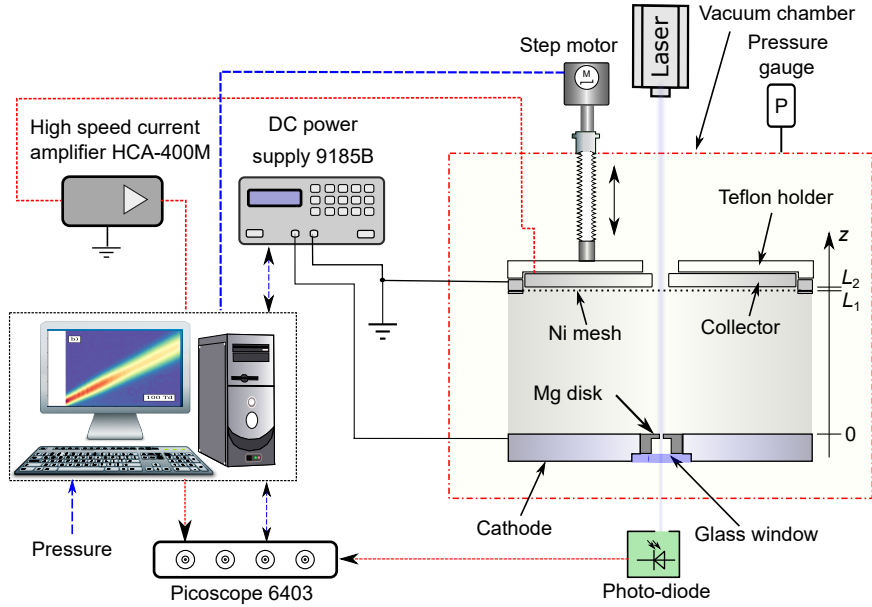


**Figure 1:** Schematic of the TOF system.

The drift cell is situated in a stainless steel vacuum chamber. The chamber is evacuated by a turbomolecular pump coupled to a rotary pump to a pressure of  $\approx 1 \times 10^{-7}$  mbar. The pressure of the gases used inside the chamber is measured by a capacitive gauge (Pfeiffer CMR 362). The experiments have been conducted with a continuous slow ( $\sim$ sccm) flow of the gas. The pressure was varied as a function of  $E/N$  (between 300 Pa (at the lowest  $E/N$ ) to 20 Pa (at the highest  $E/N$ )) in order to optimize the measured current of the drift cell, while paying attention that the applied voltage remains below the breakdown threshold over the whole range of the electrode distances covered during the scanning process.

Ultraviolet light pulses of a frequency-quadrupled diode-pumped YAG laser enter the chamber with a pulse duration of 5 ns FWHM and a repetition rate of  $\sim 3$  kHz via a feedthrough with a quartz window, traverse the grounded electrode via a hole with a diameter of 5 mm and reach the surface of a Mg disk of 5 mm diameter and 4 mm thickness, used as a photoemitter. The energy of a single pulse is  $1.7 \mu\text{J}$  (at  $\lambda = 266$  nm). The Mg disk is embedded inside the cathode of the stainless steel drift cell, which is 105 mm in diameter. The detector facing the cathode at a distance  $L_1$  consists of a grounded nickel mesh with  $T = 88\%$  ‘geometric’ transmission and 45 lines/inch density (type MN17, manufactured by Precision Eforming LLC) and a stainless steel collector electrode that is positioned at  $L_2 = L_1 + 1$  mm, i.e. 1 mm above the mesh.

Electrons generated by the laser pulses reaching the Mg disk move towards the collector under the influence of an accelerating DC voltage applied to the cathode by a BK Precision 9185B power supply. The voltage is adjusted according to the required fixed  $E/N$  value for the given experiment and the actual gap distance ( $L_1$ ) during the scanning process. The current of the detector system is generated by the moving electrons within the mesh-collector gap. The collector current is amplified by a high speed current amplifier (type Femto HCA-400M) connected to the collector, with a virtually grounded input, and is recorded by a digital oscilloscope (type Picoscope 6403B) with 0.8 ns time resolution. Data collection is triggered by a photodiode that senses the laser light pulses. Due to the low light pulse energy an averaging over typically 20 000 to 150 000 pulses is required. The experiment is fully controlled by a LabView software.

During the measurements, current traces are recorded for different values of the gap length ( $L_1$ ). The mesh and the collector are moved together by a step motor connected to a micrometer screw mounted via a vacuum feedthrough to the vacuum chamber. The distance between the mesh and the

cathode can be varied within a range of  $L_1 = 7.8 - 58.3$  mm. Within this range 53 different gap distances can be scanned over in the experiments reported here. The measurements have been carried out at a lab temperature of  $T = 20 \pm 2^\circ\text{C}$ .

Our apparatus performs the best at high  $E/N$  conditions. At low  $E/N$  we have observed low signal levels, which most likely originate from a decreasing ‘escape factor’ of the electrons from the cathode. It has been found [64], that at such conditions many of the electrons emitted from the cathode are backscattered and absorbed there after a few gas phase elastic collisions. This effect can significantly reduce the emission efficiency of the cathode. At higher  $E/N$ , where inelastic collisions also occur, these electrons cannot move back to the cathode and the ‘escape factor’ approaches a value of 1.

### 2.1.2 Data acquisition

The measured displacement current at the collector is proportional to the flux of the electrons that enter the mesh-collector gap. Under hydrodynamic conditions, i.e. when electrons reach a stationary (local equilibrium) state where the (one particle) electron velocity distribution function,  $f(\mathbf{v}, \mathbf{r}, t)$  has lost memory of its initial state and all space-time dependence is expressible through linear functionals of the electron number density,  $n_e(\mathbf{r}, t)$ , which means, that the macroscopic (transport) parameters of the swarm are space- and time-independent, the electron flux consists of two terms: the advective and diffusive component (assuming that higher spatial gradients of the electron density are negligible) [33]. The advective component is proportional to the electron density, where the proportionality factor is the flux drift velocity, and the diffusive component equals the flux diffusion tensor times the electron number density gradient [67].

Using Ramo’s theorem [68,69], it can be shown that for the experimental conditions considered in the present case, the contribution of the diffusive component to the current is negligible compared to the contribution of the advective component, except in the early stage of the swarm development when the spatial gradients of the electron number density are more significant. Therefore, we can assume, that the measured current is proportional to the electron number density, which, for a spatially infinite one dimensional (1D) system has the following analytic form [70]:

$$n_e(x, t) = \frac{n_0}{(4\pi D_L t)^{1/2}} \exp \left[ \nu_{\text{eff}} t - \frac{(x - Wt)^2}{4D_L t} \right]. \quad (3)$$

This formula is the solution of the spatially one dimensional diffusion equation and describes a Gaussian pulse in infinite space drifting in the  $x$ -direction with bulk drift velocity,  $W$ , and diffusing with respect to the centre-of-mass with the longitudinal component of the bulk diffusion tensor,  $D_L$ . Furthermore,  $n_0$  is the electron number density at the initial point (i.e.  $x = 0$ ,  $t = 0$ ), and  $\nu_{\text{eff}}$  is the effective ionization frequency (that is the difference of the ionization frequency and the attachment frequency). These transport coefficients, i.e.  $W$ ,  $D_L$  and  $\nu_{\text{eff}}$  are obtained by fitting Eq. (3) to the results of the measurements, the so-called ‘swarm maps’, which are collections of current traces, i.e. the current signal generated by electrons reaching the collector at a given gap distance, averaged over many laser pulses. A swarm map is a collection of such current traces at different gap length values (see Figure 2). From these transport coefficients the ionization coefficient,  $\alpha_{\text{eff}}$ , can also be determined by applying the relation [67]:

$$\frac{1}{\alpha_{\text{eff}}} = \frac{W}{2\nu_{\text{eff}}} + \frac{\nu_{\text{eff}}}{|\nu_{\text{eff}}|} \sqrt{\left( \frac{W}{2\nu_{\text{eff}}} \right)^2 - \frac{D_L}{\nu_{\text{eff}}}}. \quad (4)$$

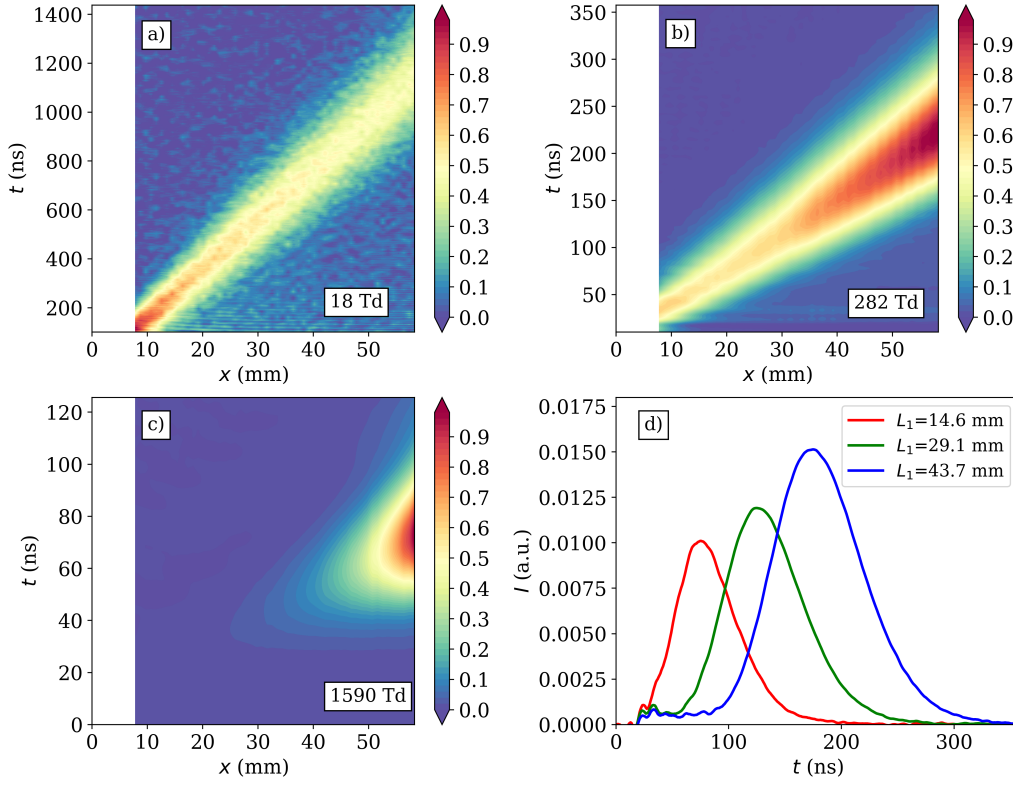


**Figure 2:** Measured swarm maps for different values of  $E/N$  in  $\text{CO}_2$  (a-c), together with vertical cuts of (b) which are the measured current traces at the gap distances given in the legend (d).

The assumption that the measured signal is proportional to the electron number density (with the analytic form of (3)) is an approximation, because the detection sensitivity to the "incoming" electrons i.e. those entering the mesh-collector gap was found to depend on the gas pressure and the collision cross sections, which both influence the mean free path of the electrons [71]. That is, a variation of the energy distribution function at different positions within the swarm (i.e. along the  $x$ -direction) may result in a distortion of the detected signal, which will then deviate from the analytical formula used to obtain the transport coefficients.

The deviation caused by this effect can be quantified by the simulation of the electrons motion in the experimental system, including the detector region. From such a simulation, one can derive the time-dependent response of the detector to the electron cloud at the same conditions as in the experiment (i.e. at the same pressure,  $E/N$ , and gap length  $L_1$ ). When this procedure is accomplished for a sequence of gap length values, a simulated swarm map can be constructed. Applying the same fitting procedure as described above for the experimental data, a new set of transport coefficients can be calculated. Now, if some kind of 'reference' transport coefficients are known, the error created by the experimental method and related assumptions in the data analysis can readily be quantified. These 'reference' transport coefficients can be obtained from independent kinetic computations, based on either the solution of the Boltzmann equation or on Monte Carlo simulation, based on cross section set for the electrons' reactions in the given gas. For this purpose, we use the cross section set of Hayashi [45]. The result of the comparison of the transport coefficients obtained from the fitting of the simulated swarm maps and the 'reference' transport coefficients is a correction factor at the given  $p$  and  $E/N$ . Repeating the above procedure for all the experimental parameter settings yields correction factors for all the experimental conditions. (We note that as the same cross section set is used in the system's simulation and in the computation of the 'reference' transport coefficients, any uncertainties in the cross sections vanish in first order.) Applying the correction factors to the experimental data yields 'Corrected' values for the measured transport coefficients which are expected to be free from the effects of the assumptions in the fitting procedure.

A low correction factor indicates that the fitting procedure using Equation (3) is correct, whereas

higher values indicate that this assumption cannot be made for the given conditions. Figure 3 shows the deviations between the simulation of the experimental system and the kinetic swarm calculations. In case of the bulk drift velocity,  $W$  (Figure 3(a)), the deviation is within 5% for the whole  $E/N$  range, and thus the determination of this transport coefficient can be taken to be reliable. The same can be stated about the effective ionization frequency,  $\nu_{\text{eff}}$  and the effective ionization coefficient,  $\alpha_{\text{eff}}$  (Figure 3(c) and (d), respectively), except for  $E/N$ -values within 100 Td and 200 Td, where the deviation rapidly grows with decreasing  $E/N$ -values. The situation is worse for the longitudinal component of the bulk diffusion tensor,  $D_L$  (Figure 3(b)). Here, the deviation ranges between  $\approx -25\%$  to  $\approx 20\%$ . The reason for this is, that this transport coefficient is determined by the spread of the measured signal, which is more susceptible to a deviation from the assumed functional form of Equation (3), as the electron energy is inhomogeneous within the swarm (electrons with higher energies tend to be in the front of the swarm, while those with lower energies tend to ‘fall behind’), thus the detection sensitivity will not be uniform for the whole swarm.

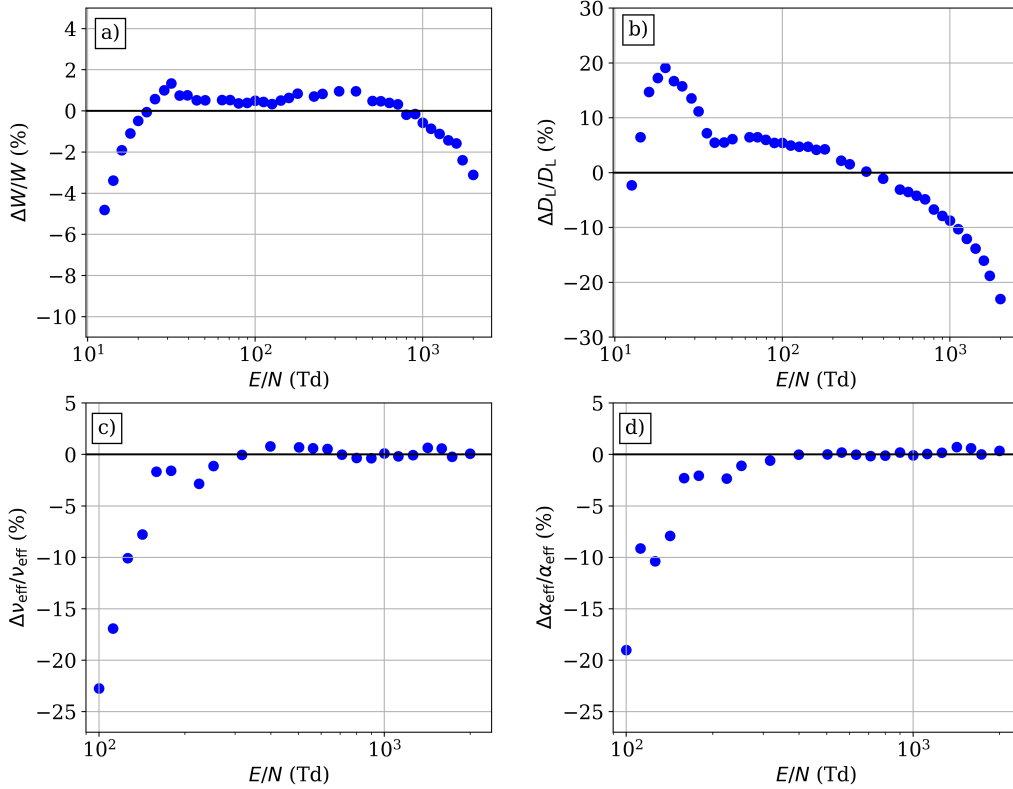


**Figure 3:** Deviations of the results between the swarm parameters obtained from the simulations of the experimental system ( $S$ ) vs. the theoretical values ( $T$ ), i.e.  $(S - T)/T$  for the bulk drift velocity (a), the longitudinal component of the diffusion tensor (b), the effective ionization frequency (c) and the effective ionization coefficient (d). Applying these correction factors to the experimental results ( $X_{\text{exp}}$ ) leads to the set of ‘Corrected’ transport coefficients ( $X_{\text{corr}}$ ) as  $X_{\text{corr}} = \frac{X_{\text{exp}}}{1 + \frac{S-T}{T}} = \frac{T}{S} X_{\text{exp}}$ .

The uncertainty of the measured data originates from (i) the finite precision of the components of the experimental system (e.g. pressure gauge, power supply, setting of the electrode gap, etc.), (ii) slightly varying external conditions (fluctuations of the laser light intensity during the course of the scanning process (typically taking 10-100 minutes), the gas pressure, the temperature of the laboratory, etc.) and (iii) the finite duration of the laser pulses and the finite noise level and response time of the measurement apparatus (amplifiers, oscilloscope, etc.) [42]. Our estimation of these results in an uncertainty for the drift velocity that is below 5%, for the longitudinal component of the diffusion tensor of  $\approx 25\%$ . For the effective ionization frequency, the uncertainty at high  $E/N$  is estimated to be in the order of  $\approx 15\%$ , which rapidly increases, when this coefficient decays orders of magnitude towards low  $E/N$  values. The errorbars shown with our experimental data express these values (only



for some measurement points the uncertainty from the fitting procedure exceeds this value) which results in the slightly bigger errorbars for these cases.

## 2.2 The Pulsed Townsend experiment

### 2.2.1 Description of the experimental setup

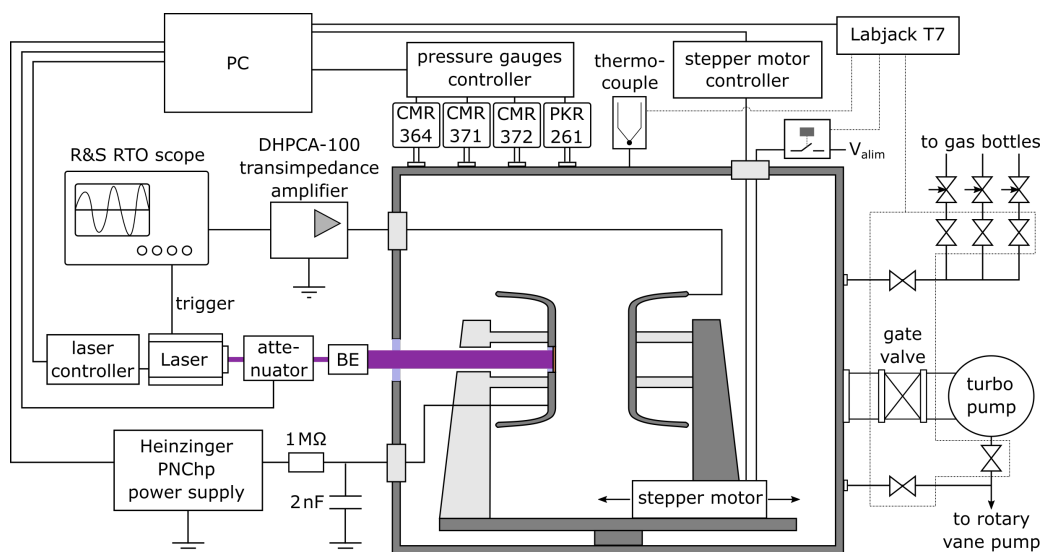


**Figure 4:** Schematic of the PT system.

The pulsed Townsend experiment has already been described in detail in previous works [36, 37], and has been used to obtain electron and ion swarm parameters in many fluorinated gases and gas mixtures [46–59] as well as in Ar, N<sub>2</sub>, CO<sub>2</sub>, O<sub>2</sub>, N<sub>2</sub>O and mixtures of those [36, 37, 60–63].

The schematic layout of the experimental apparatus can be seen in Figure 4. The electrodes are encapsulated in a 100 L stainless-steel vessel. The pressure inside the vessel is measured using the capacitive diaphragm gauges Pfeiffer CMR364, CMR371 and CMR372 which have full scale values of 100 Pa, 10 kPa and 100 kPa respectively, as well as a full range gauge PKR261. The lab temperature is regulated at 21 °C, and the temperature is measured on the external surface of the vessel with a T-type thermocouple.

When the turbo pump is running, the pressure in the vessel is about  $1 \times 10^{-5}$  Pa. Before the measurements, the pipes connecting the gas bottles are first evacuated through the vessel, and then abundantly flushed with the gas(es) under use. Then, the vessel is evacuated again and the gate valve is closed. The pressure in the vessel just before filling the gas is about  $1 \times 10^{-3}$  Pa. After filling, the valves are closed and the experiment is performed under fixed gas conditions.

The electrodes used for this experiment have a Rogowski profile, and have a total diameter of 16.5 cm. A photocathode of 2.5 cm diameter is mounted at the center of the cathode. The photocathode is made of quartz coated with two metallic layers: a 10 nm magnesium layer, topped with a 5 nm palladium layer. The photocathode is illuminated from the back with a UV laser of type FQSS 266-200 from Crylas, with a wavelength of 266 nm, a pulse duration of 1.5 ns FWHM, a pulse energy of 200 μJ and a repetition rate of 20 Hz, which releases electrons from the metallic layer. The laser beam is expanded ("BE" in figure 4) to cover about 4 cm<sup>2</sup> of the photocathode surface. The laser intensity is automatically reduced with a linear attenuator if needed to keep the total charge of the electron avalanche below 10 pC.

The emitted electrons move towards the grounded electrode under the influence of a negative DC voltage applied to the cathode using a Heinzinger PNChp power supply (either PNChp 1500 or PNChp 60000, depending on the voltage required). The electrode spacing can be adjusted with a

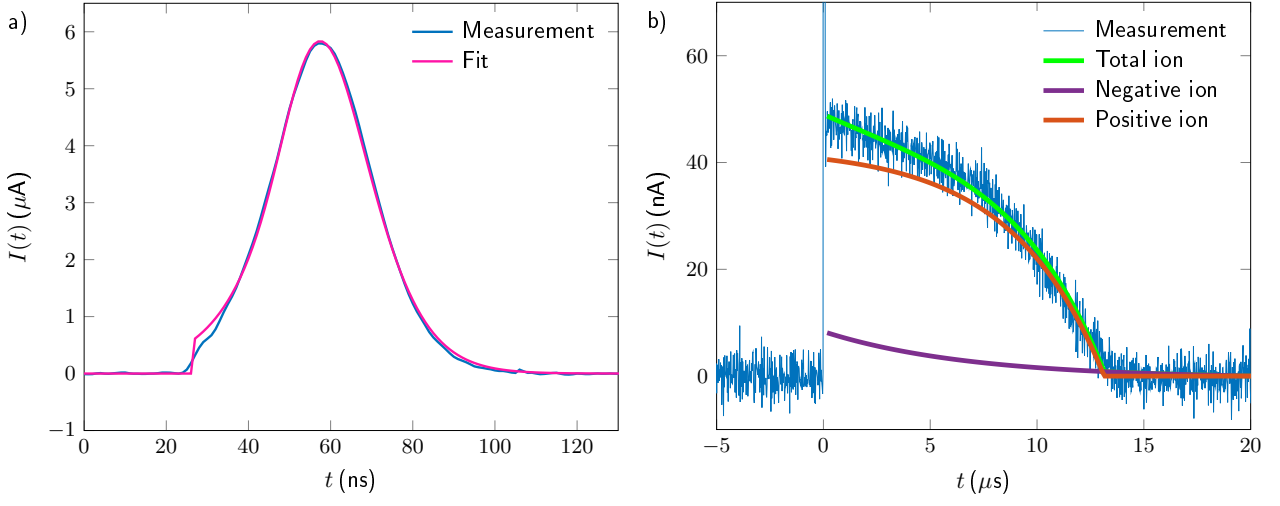


**Figure 5:** (a) Extracted electron current and fit according to equation (8). (b) Measured total current and calculated total, negative and positive ion components according to equation (9) in  $\text{CO}_2$  at  $E/N = 774 \text{ Td}$ ,  $p = 55 \text{ Pa}$  and electrode distance  $L = 20 \text{ mm}$ .

precision of  $\pm 10 \mu\text{m}$  by moving the grounded electrode with a Newport UTSPPV6 stepper motor. The displacement current is measured at the grounded electrode using a transimpedance amplifier HCA-400M-5K-C and a voltage amplifier DHPVA-200 from Femto, and a RTO 1024 oscilloscope. A capacitor of  $2 \text{ nF}$  and a resistor of  $1 \text{ M}\Omega$  are inserted between the power supply and the cathode, in order to make sure that the capacitive charging current in the circuit is negligible compared to the current induced to the electrodes by the motion of electrons and ions. The signals are averaged over approx. 200 measurements to increase the signal-to-noise ratio.

To perform a series of measurements, the change of voltage, electrode spacing and pressure is automated. For the automatic change of pressure, the gas is initially filled to the highest measuring pressure, then the pressure is automatically decreased step-wise by opening the valve to the rotary vane pump.

### 2.2.2 Data acquisition

In the PT system, the motion of the charge carriers (electrons and ions) present throughout the gap is sensed directly via the induced displacement current which flows in the outer circuit. Since electron and ion mobilities differ by orders of magnitude, the measured current is analyzed on two different timescales, nanoseconds and microseconds. Hydrodynamic conditions are assumed during the transit time of charged species. Assuming perfectly absorbing electrodes, time- and space-independent transport coefficients allow us to relate the measured displacement current to their total number via Ramo's theorem [68]:

$$I(t) = \sum_k q_0 \frac{w_k}{L} N_k(t) = \sum_k q_0 \frac{w_k}{L} \int_0^L n_k(x, t) dx, \quad (5)$$

where  $N_k$  is the number of particles of species  $k$ , drifting at constant flux velocity  $w_k$  between the electrodes of distance  $L$  [67]. In the evaluation method used in this paper, ion species are distinguished as two distinct positive and negative ion swarms with respective mobilities. On the electronic timescale, these can reasonably be assumed motionless. Hence, the temporal evolution of the positive and negative ion densities depends solely on the electron density and on the ionization or attachment event frequencies during the transit of electrons. The total current can then be expressed in terms of the electron component using equation (5) as:

$$I_{\text{tot}}(t) = I_e(t) + I_{\text{ion}}(t) = I_e(t) + \left( \nu_i \frac{w_p}{w_e} + \nu_a \frac{w_n}{w_e} \right) \int_0^t I_e(t') dt', \quad (6)$$

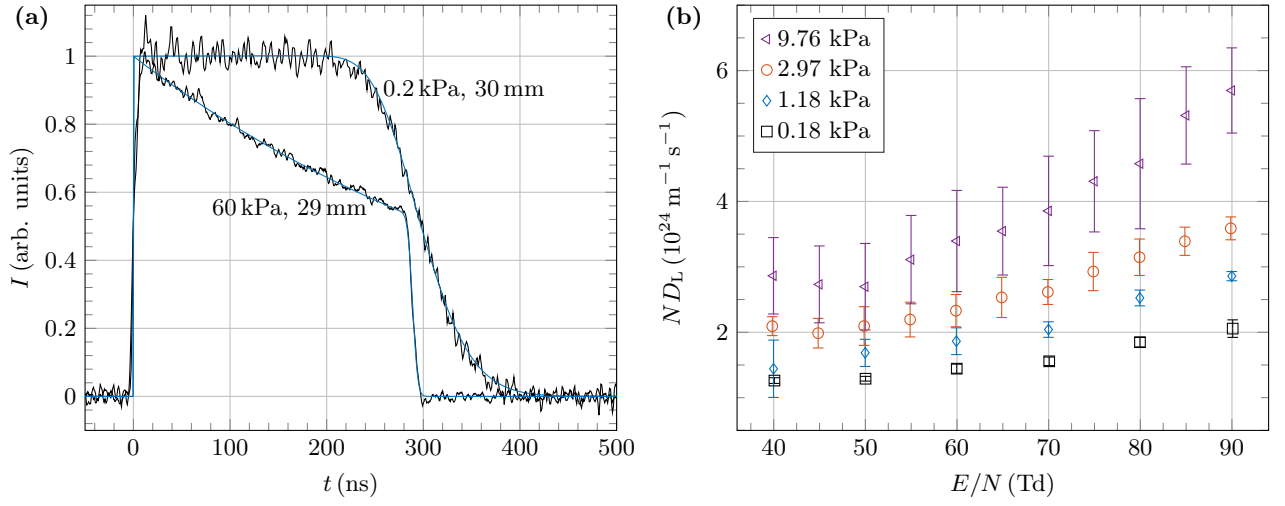


**Figure 6:** (a) Electron current in CO<sub>2</sub> at  $E/N = 40$  Td, with an electrode spacing of about 30 mm, at two different pressures: 0.2 kPa and 60 kPa. (b) Longitudinal electron diffusion coefficient derived from the measurements in CO<sub>2</sub> at different pressures (the vertical error bars reflect the uncertainty from the fitting procedure, they do not include the error due to neglecting the initial broadening of the swarm). According to the hydrodynamic approximation, the values of  $ND_L$  should be independent of pressure. Here, the values of  $ND_L$  are pressure-dependent, because neglecting the initial broadening of the swarm leads to overestimating  $ND_L$  by an amount increasing with pressure and with  $E/N$ . Therefore, the most reliable values are those obtained at the lowest pressure, here 0.18 kPa.

where  $\nu_i$ ,  $\nu_a$  are the ionization and attachment frequencies and  $w_p$ ,  $w_n$  and  $w_e$  are the positive and negative ion, and electron flux velocities, respectively. These are all unknown parameters at this point. However, it is possible to evaluate the constant in front of the integral by estimating a time  $T$  from the measurements at nanosecond timescale for which the electron current is zero, i.e. when all electrons have reached the anode. The electron current is separated by solving iteratively equation (6) starting with  $I_e^{(0)}(t) = I_{\text{tot}}(t)$  until the sequence  $I_e^{(j)}(t)$  converges:

$$I_e^{(j)}(t) = I_{\text{tot}}(t) - \left( \frac{I_{\text{tot}}(T)}{\int_0^T I_e^{(j-1)}(t') dt'} \right) \int_0^t I_e^{(j-1)}(t') dt', \quad (7)$$

where at time  $T$ ,  $I_{\text{tot}}(T) = I_{\text{ion}}(T)$ .

Assuming that all electrons are emitted at  $t = 0$  (i.e., no initial broadening of the electron cloud) the electron density is given by equation (3) and the electron current can be simply derived analytically as:

$$I_e(t) = \frac{q_0 N_e(0) w_e}{2L} \exp(\nu_{\text{eff}} t) \left( 1 - \text{erf} \left( \frac{W_e t - L}{\sqrt{4D_L t}} \right) \right), \quad (8)$$

where the bulk drift velocity and longitudinal diffusion coefficients,  $W_e$  and  $D_L$ , as well as the effective ionization frequency  $\nu_{\text{eff}} = \nu_i - \nu_a$  are obtained by fitting equation (8) to the extracted electron current waveforms of given  $E/N$  value. Strictly speaking, equation (8) is derived assuming the cathode is located at  $-\infty$ . An example of measured electron current in CO<sub>2</sub> at high  $E/N$  and its fit according to equation (8) is shown in figure 5(a).

The assumption of no initial broadening in equation (8) leads to an error (overestimation) when fitting the longitudinal diffusion coefficient  $ND_L$ . This error is negligible when the broadening of the electron swarm during the drift is much larger than the initial broadening  $\sigma_0$ , i.e.  $\sqrt{2D_L T_e} \gg \sigma_0$ , where  $T_e$  is the electron transit time given by  $L/W_e$ . The condition  $\sqrt{2D_L T_e} \gg \sigma_0$  is fulfilled at sufficiently low pressure and sufficiently large electrode spacing. The amount by which  $ND_L$  is overestimated increases with increasing  $E/N$  because the drift time  $T_e$  decreases, and it also increases with increasing gas pressure because  $D_L$  decreases. Consequently, the preferred values of  $ND_L$  are those obtained at the lowest available pressure. Figure 6(a) shows two electron currents measured

in CO<sub>2</sub> at  $E/N = 40$  Td, at two different pressures: 0.2 kPa and 60 kPa. It can be seen that the effect of the diffusion, i.e. the broadening of the signal, is much larger at 0.2 kPa than at 60 kPa. At 60 kPa, neglecting the initial broadening leads to a significant overestimation of the diffusion coefficient  $ND_L$ . Figure 6(b) shows the values of  $ND_L$  obtained at different pressures, and subject to an error because of neglecting the initial broadening. A clear increase of  $ND_L$  (and of its associated uncertainty) is visible with increasing pressure and with increasing  $E/N$ . Note that the error bars shown in figure 6(b) reflect the uncertainty on  $ND_L$  due to the fitting procedure and do not include the error due to neglecting the initial broadening.

In contrast to the diffusion coefficient  $ND_L$ , it is beneficial to measure the effective ionization coefficient  $\nu_{\text{eff}}$  at the highest possible pressure, because the uncertainty of  $\nu_{\text{eff}}/N$  is inversely proportional to the gas density  $N$ . In figure 6(a), the value of  $\nu_{\text{eff}}/N$  can be read much more accurately at 60 kPa than at 0.2 kPa, where the negative slope of the current is barely visible. Therefore, the preferred values of  $\nu_{\text{eff}}/N$  are those obtained at the highest available pressure.

Having extracted the electron transport coefficients, the positive and negative ion currents can be now derived for  $t \geq T_e$ :

$$I_p(t') = I_0 \frac{w_p}{w_e} \frac{\nu_i}{\nu_{\text{eff}}} \left( e^{\nu_{\text{eff}} T_e} - e^{\nu_{\text{eff}} \frac{T_e}{T_p} t'} \right) \quad \text{and} \quad I_n(t') = I_0 \frac{w_n}{w_e} \frac{\nu_a}{\nu_{\text{eff}}} \left( e^{\nu_{\text{eff}} T_e (1 - \frac{t'}{T_n})} - 1 \right), \quad (9)$$

where  $t' = t - T_e$ ,  $I_0 = \frac{q_0 N_e(0) w_e}{L}$  is the initial electron current and  $T_n = L/W_n$  and  $T_p = L/W_p$  the transit times of the negative and positive ion swarms. An example of calculated total, negative and positive ion currents is given in figure 5(b). The discussion of the ion transport properties is, however, not the topic of this work.

In the PT setup, the  $E/N$  values are set with an accuracy of  $\pm 0.5\%$  over a wide range of pressures (0.01 Pa ... 100 kPa  $\pm 0.15\%$ ), distances (11 mm ... 35 mm  $\pm 10 \mu\text{m}$ ) and voltages (7.5 V ... 60 kV  $\pm 0.02\%$ ) taking also into account the uncertainty on the measured room temperature and the slight inhomogeneity of the applied electric field in between the electrodes (0.2%) [36]. In the evaluation of the effective ionization rate at a set of  $(U, L, p)$ -values, the main source of uncertainty is the noise on the signal. To increase the signal to noise ratio (SNR), the measurements are repeated a large number of times (200 to 400 repetitions for  $20 \leq E/N \leq 1000$  Td and more than 1000 repetitions for  $E/N \leq 20$  Td) and only the average signal is kept for the evaluation. In addition, the photocathodes are frequently renewed to maintain a number of initial electrons above  $10^5$ . For the drift velocity and the longitudinal diffusion coefficient, an additional source of error is the limited bandwidth of the transimpedance and voltage amplifiers as well as the finite laser pulse length in the determination of the diffusion coefficient.

The high reproducibility of the measurements demonstrated in [36] allows a flexibility in choosing the appropriate range of operating conditions for which the uncertainty on the evaluated swarm parameters is the lowest as described above. To get an estimation on the accuracy of the measurement in addition to the precision, measurements at a single  $E/N$ -value are repeated for a large set of  $(U, L, p)$ -values. The standard deviation which derives from this is included in the evaluation of the errorbars and is the largest contributor for  $20 < E/N < 500$  Td.

## 2.3 Comparison of the approaches

Some key differences and limitations of the two experimental systems are highlighted in this section. Most of the time, these limitations can be prevented in the experiment itself or overcome by advanced signal analysis when they are detected and their origin is known. Because of different design goals, the two setups typically operate at different experimental conditions and with different hardware:

- **electrode diameter:** The electrode diameter should be sufficient to ensure that all electrons are collected, taking into account the transverse diffusion.
- **operating pressure:** A sufficiently low operating pressure enables measurements at elevated  $E/N$  values because the electron multiplication is limited and does not lead to electrical breakdown. In contrast, the benefit of a high operating pressure is to obtain more precise values for

the reaction rate coefficients, and to observe the drift ions, additionally to that of the electrons. By analyzing the ion current, different reaction rate coefficients can be distinguished, not only the effective ionization rate coefficient. The TOF setup was primarily designed to operate at low pressure, from a few 10 Pa to a few 100 Pa, whereas the PT was designed to operate from 1 kPa to 100 kPa. A set of measurements in the PT setup typically includes different pressures, so that the rate coefficients of two and three-body processes can be distinguished. At low pressure, the PT technique is limited by the physical condition that swarm-equilibration should be much faster than the drift time of electrons through the cell. The PT setup is limited at high pressure to 100 kPa because the experiment was not designed to have internal over-atmospheric pressure. Regarding the TOF system, the response time of the data acquisition electronics and the finite duration of the laser pulses sets the limit of operation at low pressures, while the vanishing signal level (as discussed in sec. 2) limits the operation at high pressures.

- **laser power:** The pulse energy influences the number of initial electrons in both setups. The benefit of a low pulse energy (smaller number of initial electrons) is that it is easier to avoid problems such as space charge effects, breakdown and excessive production of excited species. The benefit of high pulse energy is that less averaging (repetitions) are needed to measure the current signals. Additionally, a high number of initial electrons is required in case of gases and conditions when strong electron attachment is present. The TOF and PT setups operate at the same laser wavelength of 266 nm but with different pulse energy: 1.7  $\mu\text{J}$  per pulse for the TOF setup and adjustable from 2 to 200  $\mu\text{J}$  per pulse for the PT setup. The higher repetition rate in the TOF setup makes it easier to perform averaging over a higher number of pulses, which is necessary at the lower pulse energy of this system.
- **laser pulse length:** In both data acquisition methods the finite duration of the laser pulses is neglected. In reality, this finite duration (the time-dependent intensity during the pulse) extends the spatial size of the electron cloud, with respect to an "ideal" cloud shape that belongs to an instantaneous emission of the electrons, of which the mathematical form (3) is assumed in the data analysis in both systems. The finite duration of laser pulses of 1.5 ns and 5 ns, respectively, for the PT and TOF setups, is however, short compared to the transport time scales that are typically in the order of  $\sim 100 - 1000$  ns (see figures 2 and 6). For the TOF measurements, the possible effects of the broadening of the electron cloud has to be kept in mind at high  $E/N$  and low pressure conditions. For the PT setup, in turn, the effect of initial broadening is particularly noticeable in the evaluation of the diffusion coefficient at low electrode separation distance and higher pressure, as mentioned above in section 2.2.2.

Additionally, the two setups address differently the physical limitations of the measurements:

- **Non-hydrodynamic region:** A certain time / drift length is needed for the photoelectrons emitted from the cathode to reach the steady-state energy distribution. During this equilibration time / space, the transport parameters are not defined and there is no straightforward interpretation for the measured current. As such effects are not accounted for by the mathematical form of the spatio-temporal density distribution of the electron cloud used in the data acquisition for both systems, working under conditions that ensure a short equilibration time with respect to the transport time scale / short equilibration length with respect to the electrode gap is strongly preferred. In the swarm maps obtained from the TOF measurements nonequilibrium behavior can directly be observed [71] and excluded from the analysis. In the PT setup, in turn, this effect can neither be directly observed nor excluded. As the scanning TOF system has a minimum electrode gap defined by its construction the most sensitive region cannot be observed. Therefore, attention has to be paid in both experiments to avoid conditions with excessive equilibration time / length for the swarms. In general, nonequilibrium effects are most critical in atomic gases and at  $E/N$  values of typically few times 10 Td. In molecular gases the effect is less pronounced. Due to the pressure  $\times$  length scaling, operation at high pressures is advanta-

geous at low  $E/N$ , which favours the use of the PT system, which is more suited to work under such conditions.

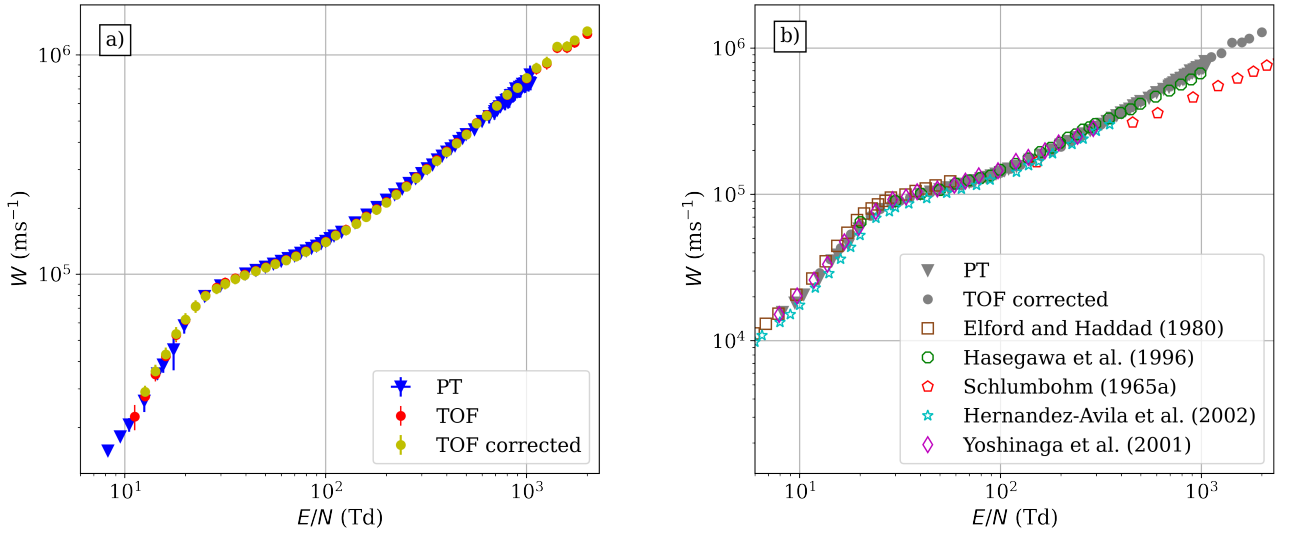
- **space charge effects:** In both setups, accumulation of space charges may distort the (otherwise) constant electric field over the electrode gap, thus it is to be avoided. The TOF setup operates with a lower number of initial electrons because of the low laser pulse energy and is thus less susceptible to this problem. In the PT setup, space charge effects are mitigated by illuminating a large area on the photocathode ( $4 \text{ cm}^2$ ), which lowers the electron density. Additionally, the total charge of the avalanches is actively regulated below  $10 \text{ pC}$  by attenuating the laser light between 1-100%. This  $10 \text{ pC}$  charge is an absolute maximum, and the vast majority of measurements have a much lower charge. This total charge corresponds to approximately  $6 \times 10^7$  charged particles, which include not only electrons, but also anions and cations produced. Therefore, the number of electrons is significantly below Meek's criterion of  $10^8$  electrons for the avalanche to streamer transition [65]. Decreasing further the total charge is feasible, but a compromise is needed between avoiding space-charge effects and maintaining a sufficient SNR ratio [62].
- **presence of excited species:** Both setups make efforts to limit the production and accumulation of excited molecules and dissociation products, which could affect the transport parameters by de facto changing the gas composition. The TOF experiment is pulsed at  $3 \text{ kHz}$  but a constant gas flow is maintained to avoid the accumulation of excited species. In contrast to this, the PT experiment uses no gas flow but operates with a slower repetition rate of  $20 \text{ Hz}$ .
- **impact of ion collisional processes:** In the present study, both the TOF and PT analysis in  $\text{CO}_2$  assume the presence of electron attachment and electron impact ionization only. Generally, this assumption should not be taken for granted. In some cases, ion collisional processes, such as an electron detachment from negative ions and ion conversion processes can significantly affect the measured current [62, 66]. The rates of ion collisional processes depend on the collision frequency for collisions between ions and neutral molecules, on the electric field strength and on the gas pressure. In conditions where these processes are significant, the numerical procedures used to analyse the current signals should be adapted to include their effects.

Additionally to all above-mentioned points, attention must be paid to unexpected measured current shapes in both experiments, as these could be indications of further limitations which were not identified, or operation outside the region of valid assumptions.

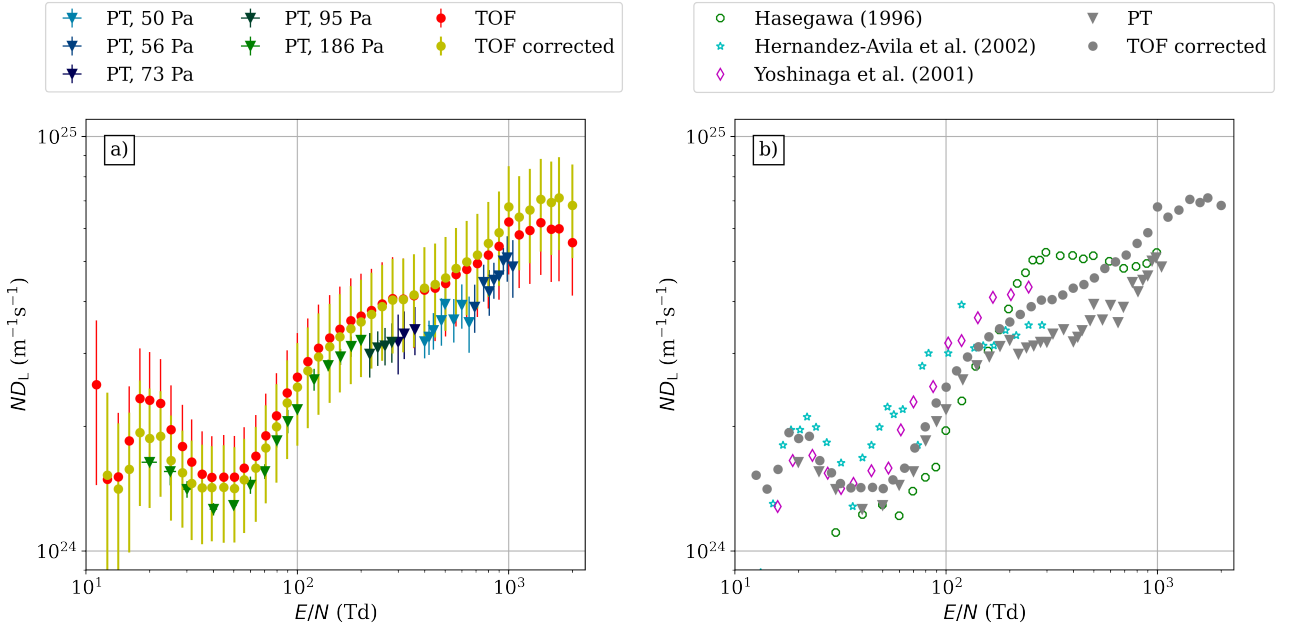
### 3 Results

In this section, results are presented for the transport coefficients (bulk drift velocity, longitudinal component of the bulk diffusion tensor, effective ionization rate coefficient and density reduced effective ionization coefficient) over a wide range of  $E/N$ -values:  $8 \text{ Td} \leq E/N \leq 2000 \text{ Td}$  for  $W$ ,  $10 \text{ Td} \leq E/N \leq 2000 \text{ Td}$  for  $ND_L$ ,  $3 \text{ Td} \leq E/N \leq 2000 \text{ Td}$  for  $\nu_{\text{eff}}/N$  and  $80 \text{ Td} \leq E/N \leq 2000 \text{ Td}$  for  $\alpha_{\text{eff}}/N$ . The data obtained by the two experimental systems are compared.

Figure 7 shows the bulk drift velocity,  $W$  for the PT experiment as well as for the TOF experiment along with the corrected values of the latter, whereby the correction method was carried out as described in section 2.1.2 (a), and their comparison to other experimental data (b). For the bulk drift velocity, this correction amounts to a few percents. The datasets from the two systems for the bulk drift velocity have very good agreement (within  $\approx 5\%$ ) over the whole overlapping  $E/N$  range.



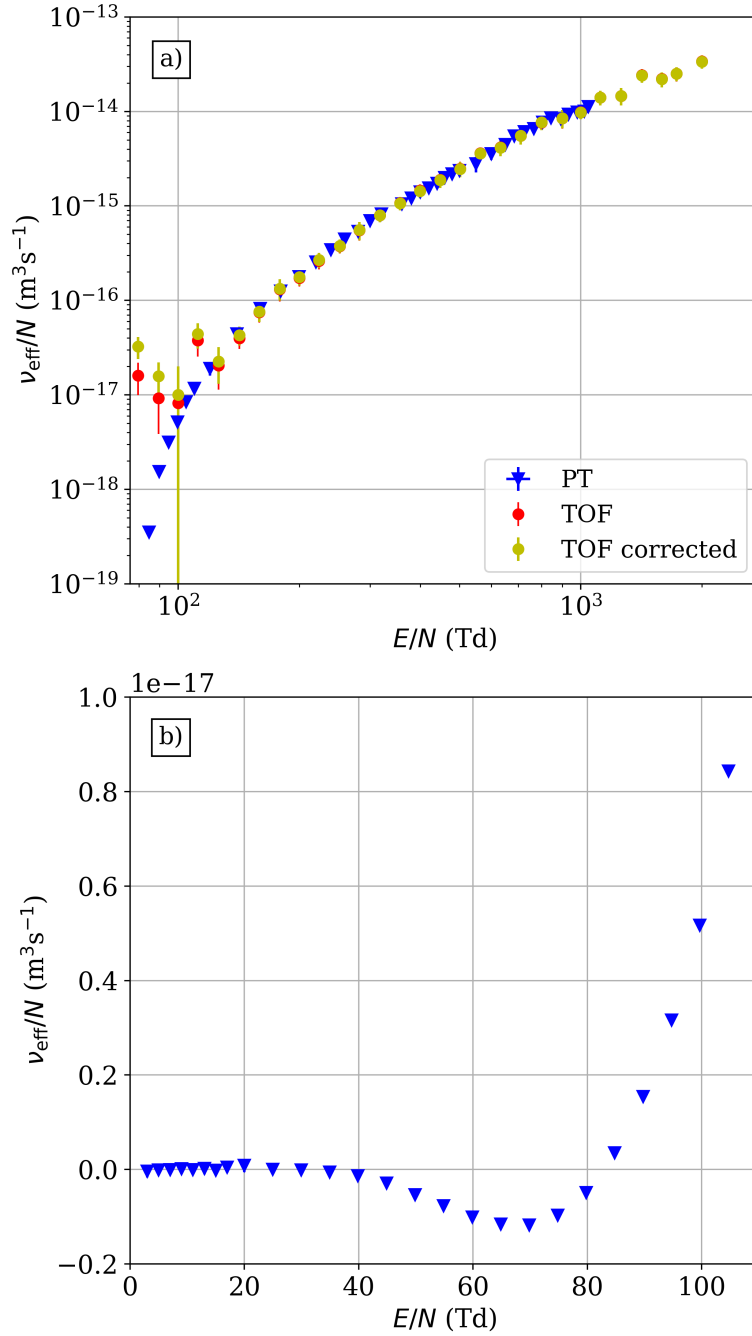
**Figure 7:** Comparison of the bulk drift velocity values ( $W$ ) obtained by the two different experimental setups (a) and comparison of these values to other experimental data (b): Elford and Haddad [72], Hasegawa *et al.* [73], Schlumbohm [74], Hernandez-Ávila *et al.* [75], Yoshinaga *et al.* [76]. For the determination procedure of the corrected experimental values in case of the TOF experiment in panel (a), see section 2.1.2. For most data points, error bars are smaller than the respective symbols.



**Figure 8:** Comparison of the measured values of the longitudinal component of the bulk diffusion tensor ( $ND_L$ ) obtained by the two experimental setups (a) and their comparison to other experimental data (b): Hasegawa *et al.* [73], Hernandez-Ávila *et al.* [75], Yoshinaga *et al.* [76]. In the TOF experiment the pressure ranged between 20 Pa (at the highest  $E/N$ ) to 300 Pa (at the lowest  $E/N$ ). The operating pressures of the PT experiment are indicated in the legend.

For the PT system, each data point corresponds to the average over 2 to 8 ( $U, L, p$ )-values and the data set extends as low as 8 Td, below which the low SNR prevents a precise evaluation of the drift velocity, and as high as 1040 Td. The TOF-experiment provides high-precision data (within a few percents) at higher  $E/N$ -values (up to 2000 Td) and as low as 12 Td. Both methods give very precise results, i.e. they scatter within percents. As for the comparison with other experimental results, our data agrees very well with the works of the other authors listed above, except for Schlumbohm [74],

who also used a PT-method to obtain transport coefficients: in this case there is an increasing deviation with increasing  $E/N$ .



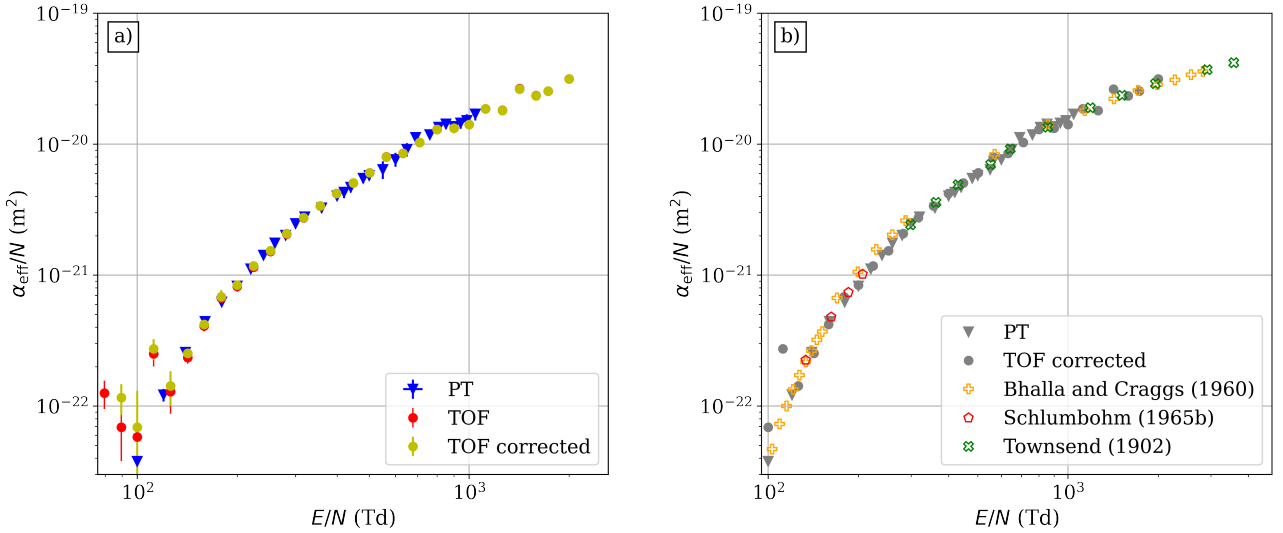
**Figure 9:** (a) Comparison of the effective ionization rate coefficient ( $\nu_{\text{eff}}/N$ ) obtained by the two experimental setups. (b) Effective ionization rate coefficient at low  $E/N$  values obtained from the PT experiment. Note the negative values that indicate the dominance of electron attachment over ionization.

Figure 8 shows the longitudinal component of the bulk diffusion tensor,  $ND_L$ . In panel (a) the two systems show a generally good agreement as the error margin of both datasets overlap. Accordingly to section 2.2.2, for each  $E/N$ -value, the result obtained with the PT system in the lowest gas-pressure is kept and given here. The discrepancies between the sets of different pressures is clearly visible in figure 8 and the scatter of the results seems to be enhanced with increasing  $E/N$ . The TOF results have a high uncertainty over the measured  $E/N$  range and increases significantly below 20 Td (as big as 100 % in some cases), therefore the determination of this transport coefficient is not reliable at such low  $E/N$  values in the TOF system. The TOF system has a wider range of measurements, i.e.



its highest  $E/N$  value is 2000 Td. Between 10 Td and 1040 Td, the  $ND_L$  values obtained by the PT system are smaller than that of the TOF system, but the two datasets show a similar trend, in particular in the range between 20 Td and 200 Td. Considering other experimental data shown in figure 8 (b), there is a reasonably good agreement between our datasets and previous measurements, especially at low and intermediate ( $20 \text{ Td} \leq E/N \leq 200 \text{ Td}$ )  $E/N$ -values. Furthermore, given the higher uncertainty of the TOF-system, the results of previous measurements are all within the uncertainty range of the TOF-system.

Figures 9 and 10 show the effective ionization rate coefficient,  $\nu_{\text{eff}}/N$ , and the density reduced effective ionization coefficient,  $\alpha_{\text{eff}}/N$ , respectively. As mentioned in section 2.2.2, the effective ionization rate coefficient obtained with the PT experiment at the highest gas pressure are shown here. The obtained results with the PT experiment have high precision over the whole  $E/N$  range, i.e. between 3 Td and 1040 Td. There is a good agreement between the two sets of data at intermediate and high  $E/N$  values, i.e. above 150 Td. Below 150 Td, the TOF system does not produce reliable results for the effective ionization rate coefficient due to the reduced SNR. As figure 9(b) reveals, electron attachment dominates ionization between  $\sim 40$  Td to  $\sim 85$  Td, as indicated by a negative  $\nu_{\text{eff}}$  value. The strongest attachment occurs at around 70 Td and vanishes as  $E/N \rightarrow 0$ . Figure 10 (b) shows the comparison of the present measurements with available experimental data for  $\alpha_{\text{eff}}/N$ . The datasets show very good agreement throughout the whole  $E/N$ -range, where data is available ( $100 \text{ Td} \leq E/N \leq 2000 \text{ Td}$ ).



**Figure 10:** Comparison of the density reduced effective ionization coefficient values ( $\alpha_{\text{eff}}/N$ ) obtained by the two experimental setups (a) and their comparison to other experimental data (b): Bhalla and Craggs [77], Schlumbohm [78], and Townsend [79].

## 3.1 Discussion

### 3.1.1 Bulk drift velocity and mobility

Both setups derived the bulk drift velocity and electron mobility in  $\text{CO}_2$  with a high precision. Furthermore, the excellent agreement of the results in the large overlapping region between 10 Td and 1000 Td confirms also the accuracy of the results. This implies that the physical assumptions underlying the analysis of both experiments are valid.

As an example, one of the physical limits of the PT setup is the non-equilibrium transport of electrons after their emission from the cathode. If the duration of the non equilibrium transport would not be negligible, the values of the bulk drift velocity would be affected. In contrast to this, the TOF experiment can exclude the non-equilibrium transport period from the analysis. The agreement

of both results confirms the physical assumption of neglecting non-equilibrium transport under the present conditions in the PT setup.

### 3.1.2 Longitudinal component of the bulk diffusion tensor

In the PT system, the obtained values of the longitudinal component of the bulk diffusion tensor are subject to an error due to the underlying assumption of no initial broadening of the electron swarm. This error was minimized by selecting the measurements performed at the lowest pressure.

In the TOF system, the obtained values of longitudinal component of the bulk diffusion tensor have overall a large uncertainty. As discussed in section 2.1, the correction procedure of the TOF system yields a greater difference at high  $E/N$  values, as due to the higher energy of the electrons the electron swarm becomes more anisotropic and hence the detector sensitivity plays a major role. At low  $E/N$  values, the values of  $ND_L$  obtained in the TOF setup are subject to a larger uncertainty due to the reduced SNR. The reduced SNR affects the ‘width’ of the signal more than the position of the maximum value. Therefore, significant uncertainties result in case of the longitudinal component of the bulk diffusion tensor, which are not present in case of the bulk drift velocity.

Despite these issues in both experiments, a reasonable agreement of the results can be observed. It seems that in the case of the longitudinal component of the bulk diffusion tensor, the PT system yields slightly more accurate at low and intermediate values of the reduced electric field, whereas the TOF system does the same at high values of  $E/N$ . In this sense, the two experimental setups complement each other.

### 3.1.3 Effective ionization rate coefficient and density reduced effective ionization coefficient

Above 150 Td, a good agreement is observed between the results of the two experiments, which confirms their accuracy. Below 150 Td the SNR in the TOF experiment is not sufficient to obtain reliable results for the effective ionization rate coefficient, and *a fortiori* for the density reduced effective ionization coefficient.

## 4 Conclusions

Electron rate and transport coefficients (bulk drift velocity,  $W$ , the longitudinal component of the bulk diffusion tensor,  $ND_L$ , effective ionization rate coefficient,  $\nu_{\text{eff}}/N$ , and density reduced effective ionization coefficient,  $\alpha_{\text{eff}}/N$ ) have been measured in  $\text{CO}_2$  by two independent experimental setups, which have been compared to each other and to previous independent measurements found in the literature. The experimental setups operate under the hydrodynamic conditions where one is a ‘scanning’ drift tube which belongs to a group of TOF experiments, whereas the other is a typical PT experiment. However, the data acquisition methods are different: in case of the TOF system, the whole spatio-temporal distribution of the density of an electron swarm for an unbound region,  $n(x, t)$  (equation (3)) is fitted to the measured displacement current, whereas in the PT system its integral over the whole spatial domain of the drift tube is fitted to the measured time dependent displacement current. The TOF results undergo a correction procedure, where the sensitivity of the detector is taken into account by comparing Monte Carlo simulation results of the experimental setup and a spatially unbounded region [44]. Both experimental systems have already been used to obtain electron transport coefficients in different gases, which were compared to other, independently measured data.

The results for the bulk drift velocity,  $W$ , showed almost perfect agreement (within  $\approx 1 - 2\%$ ) over the whole reduced electric field ( $E/N$ ) region, where both measurements have data (between 10 Td and 1000 Td). The TOF system has a wider range of reduced electric field where it can provide experimental data, up to 2000 Td. The comparison to previous measurements also showed a very good agreement except for Schlumbohm [74], where considerable deviation was observed at high  $E/N$ -values. The data obtained for the longitudinal component of the bulk diffusion tensor,  $ND_L$ , showed a generally good agreement, although the PT results are smaller than that of the TOF system

over the whole  $E/N$  range. The PT and TOF setups both show a high repeatability of results. In the PT setup, to further test the accuracy of measurements, additional measurements are performed by varying pressure and distance as much as possible while keeping the same  $E/N$  ratio. The results differ more than the repeatability at a single condition would suggest, as was already observed in a previous work [36]. This shows that high repeatability is not sufficient to warranty high measurements accuracy. At low reduced electric field values the TOF system cannot produce accurate results, as due to the small SNR the ‘width’ of the signal cannot be properly detected and thus the fitting yields a high uncertainty. The comparison with other datasets yielded reasonably good agreement at low and intermediate  $E/N$ -values (between 20 Td and 200 Td). Regarding the effective ionization rate coefficient,  $\nu_{\text{eff}}/N$  as well as the density reduced effective ionization coefficient,  $\alpha_{\text{eff}}/N$ , the results above 100 Td agree within a few percents. Likewise, the agreement is very good between the present results and previous measurements. Below this threshold, the TOF system cannot produce reliable results, but it extends the  $E/N$  range in the direction of higher values, up to 2000 Td. Consequently, it can be stated, that the TOF system gives accurate results for a wide range of reduced electric field values, but at small values (below 10 Td for  $ND_L$  and 100 Td for  $\nu_{\text{eff}}/N$  and  $\alpha_{\text{eff}}/N$ ), due to the small SNR, the data obtained are either not reliable or have high uncertainties. For gases such as  $\text{CO}_2$ , which do not strongly attach electrons, the PT setup preferably operates below 1000 Td, whereas the TOF system’s maximal value is 2000 Td. In the overlapping region, i.e. at intermediate  $E/N$  values the agreement of the data obtained by the two experimental systems indicate the correctness of the measured electron transport coefficients.

## Acknowledgments

Support by the Hungarian Office for Research, Development and Innovation (NKFIH) grants K119357, K132158, by the ÚNKP-19-3 New National Excellence Program of the Hungarian Ministry for Innovation and Technology, and by the Deutsche Forschungsgemeinschaft (DFG, German Research Foundation), project number 327886311, is gratefully acknowledged. The Zurich group acknowledges financial support from GE Grid (Switzerland) GmbH, ABB Switzerland Ltd and Siemens AG. DB and SD are supported by the Ministry of Education, Science and Technological Development of the Republic of Serbia and the Institute of Physics (Belgrade).

## References

- [1] Petrović Z L, Šuvakov M, Nikitović Ž, Dujko S, Šašić O et al. 2007 *Plasma Sources Sci. Technol.* **16**(1) S1
- [2] Yu Q, Kong M, Liu T, Fei J, Zheng X et al. 2012 *Plasma Chem. Plasma Process.* **32** 153-163
- [3] Li R, Tang Q, Yin S and Sato T 2007 *J. Phys. D: Appl. Phys.* **40** 5187-5191
- [4] Li R, Tang Q, Yin S and Sato T 2007 *Appl. Phys. Lett.* **90** 131502
- [5] Wang S, Zhang Y, Liu X and Wang X 2012 *Plasma Chem. Plasma Process.* **32** 979-989
- [6] Fridman A 2008 *Plasma Chemistry* (Cambridge University Press, New York)
- [7] Scarduelli C, Guella D, Ascenzi D and Tosi P 2011 *Plasma Processes Polym.* **8** 25-31
- [8] De Bie C, Martens T, van Dijk J, Paulussen S, Verheyde B et al. 2011 *Plasma Sources Sci. Technol.* **20** 024008
- [9] Snoeckx R, Aerts R, Tu X and Bogaerts A 2013 *J. Phys. Chem. C* **117** 4957-4970
- [10] Fidalgo B, Dominguez A, Pis J and Menedez J 2008 *Int. J. Hydrogen Energy* **33** 4337-4344

- [11] Bo Z, Yan J, Li X, Chi Y and Cen K 2008 *Int. J. Hydrogen Energy* **33** 5545-5553
- [12] Bogaerts A, De Bie C, Snoeckx R and Kozák T 2017 *Plasma Processes Polym.* **14**(6) 1600070
- [13] Mei D, Zhu X, He Y, Yan J D and Tu X 2015 *Plasma Sources Sci. Technol* **24** 015011
- [14] Ozkan A, Dufour T, Arnoult G, De Keyzer P, Bogaerts A et al. 2015 *J. CO2 Util.* **9** 74
- [15] Aerts R, Somers W, and Bogaerts A 2015 *ChemSusChem.* **8** 702
- [16] Ramakers M, Michielsens I, Aerts R, Meynen V and Bogaerts A 2015 *Plasma Process. Polym.* **12** 755
- [17] Bongers W, Bouwmeester H, Wolf B, Peeters F, Welzel S et al. 2017 *Plasma Processes Polym.* **14**(6) 1600126
- [18] Spencer L F and Gallimore A D 2013 *Plasma Sources Sci. Technol* **22** 015019
- [19] Silva T, Britun N, Godfroid T and Snyders R 2014 *Plasma Sources Sci. Technol* **23** 025009
- [20] Lee H and Sekiguchi H 2011 *J. Phys. D: Appl. Phys.* **44** 274008
- [21] Tu X and Whitehead J C 2014 *Int. J. Hydrogen Energy* **39** 9658
- [22] Liu J L, Park H W, Chung W J and Park D 2016 *Chem. Eng. J.* **285** 234
- [23] Zhu B, Li X S, Shi C, Liu J L, Zhao T L et al. 2012 *Int. J. Hydrogen Energy* **37** 4945
- [24] Zhu B, Li X S, Liu J L, Zhu X and Zhu A M 2015 *Chem. Eng. J.* **264** 445
- [25] Ruiz-Vargas G, Yousfi M and de Urquijo J 2010 *J. Phys. D: Appl. Phys.* **43** 455201
- [26] Grofulović M, Alves L L and Guerra V 2016 *J. Phys. D: Appl. Phys.* **49** 395207
- [27] Guerra V, Silva T, Ogloblina P, Grofulović M, Terraz L, da Silva M L, Pintassilgo C D, Alves L L and Guaitella O 2017 *Plasma Sources Sci. Technol.* **26** 11LT01
- [28] Jawad E A and Jassim M K 2019 *Energy Procedia* **157** 117-127
- [29] Attie D 2009 *Nucl. Instrum. Meth. Phys. Res. A* **598** 89–93
- [30] Korolov I, Vass M, Bastykova N K and Donkó Z 2016 *Rev. Sci. Instrum.* **87**(6) 063102
- [31] Huxley L G H and Crompton R W 1974 *The Diffusion and Drift of Electrons in Gases* (New York: Wiley)
- [32] Berghöfer Th, Blümer J and Hörandel J R 2004 *Nucl. Instrum. Methods Phys. A* **525** 544
- [33] Robson R E 1991 *Aust. J. Phys.* **44** 685
- [34] Nakamura Y 1987 *J. Phys. D: Appl. Phys.* **20** 933-938
- [35] Hasegawa H, Date H and Shimozuma M 2007 *J. Phys. D: Appl. Phys.* **40** 2495
- [36] Haefliger P and Franck C M 2018 *Rev. Sci. Instrum.* **89**(2) 023114
- [37] Dahl D A, Teich T T and Franck C M 2012 *J. Phys. D: Appl. Phys.* **45** 485201
- [38] Bekstein A, de Urquijo J, Ducasse O, Rodríguez-Luna J C and Juárez A M 2012 *Journal of Physics: Conference Series* **370** 012006

- [39] de Urquijo J, Arriaga C A, Cisneros C and Alvarez I 1999 *J. Phys. D: Appl. Phys.* **32** 41
- [40] Tagashira H, Sakai Y and Sakamoto S 1977 *J. Phys. D: Appl. Phys.* **10** 1051
- [41] Malović et al. 2003 *Plasma Sources Sci. Technol.* **12** S1-S7
- [42] Korolov I, Vass M and Donkó Z 2016 *J Phys. D: Appl. Phys.* **49**(41) 415203
- [43] Vass M, Korolov I, Loffhagen D, Pinhao N and Donkó Z 2017 *Plasma Sources Sci. Technol.* **26**(6) 065007
- [44] Pinhao N, Loffhagen D, Vass M, Hartmann P, Korolov I, Bošnjaković D, Dujko S, Donkó Z 2020 *Plasma Sources Sci. Technol.* accepted, <https://doi.org/10.1088/1361-6595/ab7841>
- [45] Hayashi M 1990 *Electron collision cross sections determined from beam and swarm data by Boltzmann analysis* (Nonequilibrium Processes in Partially Ionized Gases ed Capitelli M and Bardsley J N) (New York: Plenum) pp 333-40
- [46] Hösl A, Pachin J, Egüz E, Chachereau A and Franck C M 2020 *IEEE Transactions on Dielectrics and Electrical Insulation* **27**(1) 322-324
- [47] Pachin J, Hösl A and Franck C M 2019 *J. Phys. D: Appl. Phys.* **52**(23) 235204
- [48] Hösl A, Chachereau A, Pachin J and Franck C M 2019 *J. Phys. D: Appl. Phys.* **52**(23) 235201
- [49] Egüz E A, Chachereau A, Hösl A and Franck C M 2019 *21st International Symposium on High Voltage Engineering* pp. 492-503 Springer, Cham.
- [50] Chachereau A, Hösl A and Franck C M 2018 *J. Phys. D: Appl. Phys.* **51** 335204
- [51] Chachereau A and Franck C M 2018 *22nd International Conference on Gas Discharges and their Applications*
- [52] Zawadzki M, Chachereau A, Kočišek J, Franck C M and Fedor J 2018 *J. Chem. Phys.* **149**(20) 204305
- [53] Hösl A, Pachin J, Chachereau A, Kornath A and Franck C M 2018 *J. Phys. D: Appl. Phys.* **52**(5) 055203
- [54] Chachereau A, Hösl A and Franck C M 2018 *J. Phys. D: Appl. Phys.* **51**(33) 335204
- [55] Chachereau A and Franck C M 2017 *20th International Symposium on High Voltage Engineering*
- [56] Chachereau A and Franck C M 2017 *J. Phys. D: Appl. Phys.* **50**(44) 445204
- [57] Chachereau A and Franck C M 2016 *J. Phys. D: Appl. Phys.* **49**(37) 375201
- [58] Chachereau A, Fedor J, Janečková R, Kočišek J, Rabie M and Franck C M 2016 *Plas. Sour. Sci. Technol.* **25**(4) 045005
- [59] Chachereau A and Franck C M 2015 *32nd International Conference on Phenomena in Ionized Gases*
- [60] Haefliger P and Franck C M 2019 *J. Phys. D: Appl. Phys.* **52**(2) 025204
- [61] Hösl A, Pachin J, Egüz E, Chachereau A and Franck C M 2019 *J. Phys. D: Appl. Phys.* **53**(13) 135202
- [62] Haefliger P, Hösl A and Franck C M 2018 *J. Phys. D: Appl. Phys.* **51**(35) 355201

- [63] Hösl A, Haefliger P and Franck C M 2017 *J. Phys. D: Appl. Phys.* **50**(48) 485207
- [64] Phelps A V and Petrovic Z L 1999 *Plasma Sources Sci. Technol.* **8**(3) R21
- [65] Meek J M 1940 *Phys. Rev.* **57**(8) 722-728
- [66] Wetzler J M and Wen C 1991 *J. Phys. D: Appl. Phys.* **24** 1964-1973
- [67] Blevin H A and Fletcher J 1984 *Aust. J. Phys.* **37** 593
- [68] Ramo S 1939 *Proc. IRE* **27** 584
- [69] Sirkis M D and Holonyak N Jr 1966 *Am. J. Phys.* **34** 943
- [70] Kumar K, Skullerud H R and Robson R E 1980 *Aust. J. Phys.* **33** 343
- [71] Donkó Z, Hartmann P, Korolov I, Jeges V, Bošnjaković D and Dujko S 2019 *Plasma Sources Sci. Technol.* **28** 095007
- [72] Elford M T and Haddad G N 1980 *Aust. J. Phys.* **33** 517-30
- [73] Hasegawa H, Date H, Shimosuma M, Yoshida K and Tagashira H 1996 *J. Phys. D: Appl. Phys.* **29** 2664
- [74] Schlumbohm H 1965 *Z. Phys.* **182** 317-27
- [75] Hernández-Ávila J L, Basurto E and de Urquijo J 2002 *J. Phys. D: Appl. Phys.* **35** 2264-9
- [76] Yoshinaga S-I, Nakamura Y and Hayashi M 2001 A measurement of temperature dependence of electron transport parameters in CO<sub>2</sub> *Proc. 25th ICPIG* **3**, 285-6
- [77] Bhalla M S and Craggs J D 1960 *Proc. Phys. Soc.* **76** 369
- [78] Schlumbohm H 1965 *Z. Phys.* **184** 492-505
- [79] Townsend J S 1902 *Philos. Mag.* **3** 557-76